Zinc Oxide and Gold Nanoparticles Synthesized via Black Carrot Root Extract: A Dual-Action Strategy Against Bacterial Pathogens and A549 Lung Cancer Cells

Mohamed Imath[1,3*], Suresh Velayudam[1,3], Sathyanathan Viswanathan[2,3], Jeslin Devadhas, Naveen Mahendiran[2,3], Lishandhini Vengatesan[5], Divyabharathi Deenadhayalan[5]

[1]Department of Pharmacology, JKKMMRF'S Annai JKK Sampoorani Ammal College of Pharmacy, Komarapalayam, Namakkal, Tamil Nadu, India.

[2]Department of Pharmacognosy, Apollo College of Pharmacy, Melaloorkuppam, Kanchipuram, Tamil Nadu, India.

[3]Department of Pharmacy, The Tamil Nadu Dr M G R Medical University, Guindy, Tamil Nadu, India.

[4]Associate Professor, School of Pharmacy, Sri Balaji Vidyapeeth (Deemed to be University), Shri Sathya Sai Medical College and Research Institute, Ammapettai, Chennai- 603108.

[5]Faculty of Pharmacy, Sree Balaji Medical College and Hospital Campus, Bharath Institute of Higher Education & Resaerch, Chrompet, Chennai.

***Corresponding author**

DOI: https://dx.doi.org/10.47772/IJRISS.2025.907000404

Received: 12 July 2025; Accepted: 18 July 2025; Published: 20 August 2025

ABSTRACT

Zinc oxide nanoparticles (ZnONPs) and gold nanoparticles (AuNPs) have gained a lot of attention in the pharmaceutical industry and have become a prominent metal oxide in biomedical applications, particularly in the area of anticancer and antibacterial therapy. In the present study, the green synthesis of novel nanomaterial by using root extract of black carrot (DC) (*Daucus carota* ssp. Sativus var. Atrorubens Alef.), ZnONPs, and AuNPs has been reported. The characterisation of DC-ZnONPs and DC-AuNPs is carried out through the physicochemical analysis following the estimation of its antibacterial and anticancer activity. The physicochemical data supports the successful characterisation of both the nanomaterial separately. Further, the study evaluated the antibacterial effect against *Escherichia coli, Pseudomonas aeruginosa, Staphylococcus aureus, and Bacillus subtilis* through well diffusion method and susceptibility assay through minimum inhibitory concentration (MIC) determination. And the anticancer effect has been determined through the detection of nuclear condensation and measurement of intracellular ROS with or without the presence of nanoparticles in lung cancer cell line. DC-ZnONPs induced 50% inhibitory concentration (IC_{50}) in A549 cells at 12.40 µg/mL which is much lower than the other two groups along with the standard. Similarly, DC-AuNPs induced 50% inhibitory concentration (IC_{50}) in A549 cells at 11.62 µg/mL while the DC root extract was 33.77 µg/mL. The effective MIC_{50} in bacterial culture were observed at 6.15, 6.4, 7.31, and 5.2 µg/mL of DC-ZnONPs and 9.3, 5.4, 5.95 and 7.57 µg/mL of DC-AuNPs. This study concluded that the synthesis of DC-ZnONPs and DC-AuNPs is easily prepared with low cost, non-toxic, and eco-friendly method. Its cytotoxic action on A549 cells and their antibacterial characteristics on pave the way to be an alternative therapy for lung cancer and bacterial infection.

Keywords: Zinc oxide nanoparticle, Gold nanoparticle, Black carrot, Anti-bacterial, Anti-cancer.

INTRODUCTION

Modern living is made easier by advances in nanoscience and nanotechnologies, which have influenced nearly

every branch of science [1]. The efficient dispersal of antimicrobials by metallic nanoparticles contributed to improved targeting and metabolism. Additionally, it has been shown that metallic nanoparticles have antibacterial qualities and can also greatly improve the antibacterial activity of natural compounds [2]. The significant growth has been seen with silver nanoparticle, gold nanoparticle, copper oxide nanoparticle, zinc oxide nanoparticle, and titanium nanoparticle with their respective anti-inflammatory, anti-bacterial, and anti-cancer activities [3,4]. Also, one of the new strategies developed to improve antimicrobial drug penetration, distribution, targeting, and metabolism is the application of drug NPs formulations [5]. Zinc oxide nanoparticles (ZnONPs) and gold nanoparticles (AuNPs) seems to have a strong resistance against microbes, and some studies indicate that they have significant antibacterial activity [6–9]. Moreover, ZnONPs and AuNPs can be chosen as biocompatible and biodegradable nanoplatforms, and their potential for treating cancer can also be evaluated previously [10–13]. It was shown that following ZnONPs therapy, the inflammatory indicators interleukin-1 (IL-1α) and CRP were also significantly reduced, while the levels of blood antioxidant enzyme (PON-1) and nitric oxide (NO) increased in diabetic rats concurrently (Jiang et al., 2018). ZnONPs produced through the green synthesis approach are reasonably priced, non-toxic, naturally biodegradable [14,15], and have a wide range of applications in medicine, including antibacterial activity against a variety of pathogens, anti-inflammatory properties, and potential anticancer properties [16]. On the other hand, AuNPs reported to modulate microRNA-155-5p in triple-negative breast cancer cells, thereby reducing interferon-γ-induced SOCS1 expression and NF-κB p65/50 activity [17].The substantial number of bioactive substances found in black carrots makes them more considerable for the green synthesis of ZnONPs and AuNPs [18]. A study that demonstrated the usage of lyophilized powdered aqueous black carrot anthocyanins at concentrations ranging from 0.0 to 2.0 mg/mL inhibited the proliferation of HT-29 and HL-60 cancer cells further corroborated this. The researchers concluded from their experiments that black carrot extract, either independently or in combination with anticancer treatments, could potentially serve as a viable alternative therapeutic approach for addressing a range of human tumours that demonstrate poor response to chemotherapy [Akhtar et al., 2017]. *Daucus carota* ssp. Sativus var. Atrorubens Alef., commonly referred to as purple carrot or black carrot, is a good source of soluble phenols, thiamine, riboflavin, niacin, folic acid, and alpha-tocopherol in addition to carbohydrates (with a clear prevalence of non-reducing sugars), minerals, and vitamins [19]. The anthocyanin pigments present in black carrots showed the significant chemo preventive effect [20]. In recent years, a significant concern for the healthcare system is the rise of bacterial infections as well as rise in cancer incidence. During therapy, many antibiotics are given either immediately before or after antineoplastic agents because bacteria like *Escherichia coli*, *Pseudomonas aeruginosa*, and *Staphylococcus aureus* frequently colonize and cause infections in cancer patients. As a result, appropriate cytostatic therapy combined with antimicrobial therapy can prolong the life of patients with certain malignant diseases [21]. Our investigation of *Daucus carota* potential for nano formulation revealed that numerous phytochemicals with antibacterial and anticancer effects are present in its root. Also, to the best of our knowledge, this plant's parts haven't been utilized for nano formulation before. We used DC root extract to synthesize DC-ZnONPs and DC-AuNPs. DC root extract served as both reducing agent and a capping agent in the synthesis of DC-ZnONPs and DC-AuNPs. The characterisation of the synthesized nanomaterials was done through physicochemical techniques such as fourier transform infrared spectroscopy (FTIR), transmission electron microscopy (TEM), dynamic light scattering (DLS), UV–vis spectroscopy, and zeta potential. The evaluation of antimicrobial and anticancer properties was conducted on gram-positive and gram-negative bacterial strains, as well as on normal osteoblasts and A549 cells (human lung cancer cells). This assessment involved cytotoxicity assays, measurements of intracellular reactive oxygen species (ROS), and DAPI staining techniques. We believe that by utilizing natural resources like DC roots together with microorganisms like bacteria, fungi, algae, might reduce the use of harmful compounds and may establish a novel antibacterial and anticancer agent.

MATERIALS AND METHODS

Materials

Materials and Methods

Zinc nitrate Zn $(NO_3)_2$, gold chloride (HAuCl4), Dulbecco's modified Eagle's medium (DMEM), 2′,7′-

dichlorodihydrofluorescein diacetate (H2DCFDA reagent), 3-(4,5-dimethylthiazol-2-yl)-2,5-diphenyl tetrazolium bromide (MTT reagent) were purchased from Sigma-Aldrich. Media for microbiology analysis and Phosphate buffer salt (Na2HPO4) and (NaH2PO4) were supplied from HIMEDIA. Human lung cancer cells (A549-code: CRM-CCL-185) and normal human primary osteoblasts (code: hFOB 1.19-CRL-3602) were purchased from the National Centre for Cell Science (NCCS), Pune, India. Double-distilled water was used as the aqueous medium for all experiments. All buffers were filtered with 0.2 µm filter paper immediately post-preparation.

Methods

Preparation of the aqueous root extract

The roots were chopped into small pieces after repeatedly washing with distilled water to eliminate impurities. Crush it in a pestle and mortar with 50 mM phosphate buffer (pH 7.4), and kept in an ice-packed tray to avoid protein denaturation. Filter it and then transferred to a fresh tube and the aqueous solution was stored at 40°C for further experiments.

Synthesis of DC-ZnONPs and DC-AuNPs

In-vitro synthesis of DC-ZnONPs was achieved by adding various doses of DC root extract (0.4, 0.6, 0.8, and 1 mL) to a 3 ml reaction mixture containing 1mM aqueous zinc salt solution, and PBS (pH 7.4). The resulting mixture was maintained at 40°C for 96 h. During incubation, the colour of the solution changed from purple to yellow, indicating that the reaction is completed. The mixture was filtered through a syringe filter and then precipitated with 100% ethanol too extract the unbound proteins. Store the synthesised nanomaterial at 4°C for additional testing. While the reduction process was used to synthesise DC-AuNPs from 1 mM aqueous gold solution, respectively. A 3 mL reaction mixture containing various doses of root aqueous extract solution (0.5, 1.0, 1.5, and 2.0 mL) and 1.0 mM HAuCl4 salt (in Separate Eppendorf) in PBS (50 mM, pH 7.4) was kept at 40 °C for 24 h. During incubation, the colour of the solution changed from brown to ruby red (AuNPs), indicating that the reaction was complete. Following filtration using a syringe filter, the mixture was precipitated with 100% ethanol to separate the unbound proteins. Finally, the synthesised nanoparticles were stored at 4°C until further testing [22].

Characterisation of novel nanomaterials

For the characterisation of DC-ZnONPs and DC-AuNPs, we used UV–visible spectroscopic method by UV-2400PC Series, Shimadzu, Japan, to measure the surface plasmon resonance (SPR) in the 200–800 nm wavelength range. This method takes advantage of the colour-changing characteristic coming from the reduction of metal salts to biosynthesised nanoparticles. The hydrodynamic radius of the produced nanoparticles was determined through dynamic light scattering (DLS) (ZEN3600 Malvern Instrument Ltd., Malvern, UK) method which evaluate the particle size and zeta potential. Moreover, transmission electron microscopy (TEM) micrograph was used to look more closely at the morphological characteristics and dimensions of the biosynthesised DC-ZnONPs and DC-AuNPs. In brief, droplet of the DC-ZnONPs and DC-AuNPs mixture was dried separately and positioned on a TEM copper grid. Filter paper was used to eliminate any extra solution. Next, using a Tenchi G2 Spirit TEM fitted with a BioTwin lens setup, the morphological characteristics and shape of the DC-ZnONPs were measured. An 80 kV fast-tracking voltage was used for the TEM study. By visualising and determining the size and morphology of the biosynthesised DC-ZnONPs, this TEM investigation offered important insights into their structural properties. FTIR spectroscopy [PerkinElmer spectrum] was applied to better insight into the interactions between proteins and nanoparticles. It was discovered that the synthesised nanoparticle's surfaces have unique functional groups. The spectrum was collected between 450 and 4000 cm−1 [23,24].

Antibacterial activity of DC-ZnONPs and DC-AuNPs

It has been estimated through the minimum inhibitory concentration (MIC) technique and well diffusion technique. The disc diffusion method was used to determine the antibacterial properties of DC root aqueous

extract, DC-ZnOPs, and DC-AuNPs. For antibacterial assay analysis, pure cultures of *Pseudomonas aeruginosa* (ATCC 2036), *Escherichia coli* (ATCC 25923), *Bacillus subtilis, and Staphylococcus aureus* (MTCC 1305) were obtained from Apollo College of Pharmacy. The strain suspension was transferred to the Mueller Hinton (M.H.) agar surface for the primary research, using overnight TSB cultures. Triplicates of 80 µL of DC-ZnONPs, 50 µL of DC-AuNPs, and DC root extract (80 µL and 50 µL) were added, along with PBS (negative control) and Levofloxacin drug (50µg). The plates were then incubated at 37◦C for the entire night. Subsequently, the inhibitory zone identified [25](Rizvi et al., 2011). For the minimum inhibitory concentrations (MICs), in 96-well microtiter plates, nanoparticles were diluted gradually using Tryptic Soy Broth (TSB) medium to provide an array of concentrations of DC-ZnONPs (1–100 µg/mL), DC-AuNPs (0.1–120 µg/mL) and Standard drug levofloxacin (0.1-100µg/mL). After the standard tested bacteria were cultivated in TSB medium for an entire night, their optical densities were adjusted to 600 of 0.4 (2×10^5 CFU/mL) for every well-received aliquot (10 µL). Following a 24-hour incubation period at 37°C and the viability counting of bacterial cells in each well, the lowest dosages of DC root extract, DC-ZnONPs, and DC-AuNPs that suppressed the growth of bacteria were found to be the MICs. The lowest concentrations of DC root extract, DC-ZnONPs, and DC-AuNPs that prevented bacterial growth were determined to be the minimum inhibitory concentrations (MICs). This assessment was conducted after incubating the samples for 24 hours at 37°C and enumerating the viable cells in each well [25].

Anticancer activity of DC-ZnONPs and DC-AuNPs

The anticancer activity has been assessed through cytotoxicity analysis through MTT assay, nuclear condensation by 4,6-Diamidino-2-phenylindole staining (DAPI staining), and intracellular ROS measurement by using DCFDA stain.

Cytotoxicity analysis

The cytotoxic potential of the synthesized nanoparticles was evaluated against both the cell lines, that is A549 cells and normal osteoblast cells through MTT assay. The cells were plated in a 96-well plate with 1×10^4 cells per well and incubated at 37°C for 24 hours. After that, DC-ZnONPs, DC-AuNPs, and DC root extract were added to A549 cells in triplicate at different concentrations, and the cells were incubated for 48 hours. Every well on the plates was treated with 5 mg/mL of MTT reagent after the plates had been incubated for 4 hours. Afterwards, DMSO was added to each well to dissolve the formazan crystals. To determine the vitality of the cells, the optical density (OD) at 570 nm was measured using a microplate reader (BIORAD-680) and a reference filter set to 655 nm (Iram et al., 2017).

Detection of nuclear condensation by DAPI staining

The apoptotic potential of DC-ZnONPs, DC-AuNPs, and DC root extract at IC_{50} levels in cancer and normal cell lines was assessed using the fluorescent nuclear dye DAPI (4, 6-diami dino-2-phenylindole). An inverted fluorescent microscope (Nikon ECLIPSE Ti-S, Japan) was used to capture images of labelled cells. J-image software assessed the fluorescence intensity of cancer cells treated with DC-ZnONPs, DC-AuNPs, and DC root extract in IC_{50} compared to untreated cells. The standard deviations and mean signal intensities were computed for a minimum of 50 treated cells [26].

Intracellular ROS generation

The measurement of intracellular ROS in treated and untreated cancer cells was dyed to fluorogenic reagent H2DCFDA with DC root extract, DC-ZnONPs, DC-AuNPs, and at IC_{50} for 48 hours at 37°C. The fluorescence intensity of DC root extract, DC-ZnONPs, and DC-AuNPs (IC_{50} treated cancer cells was compared to untreated cells using the J-image software. For a minimum of 50 treated cells, the mean signal intensity and standard deviation were determined [26].

RESULTS

Characterisation of the synthesised nanomaterials

The aqueous root extract of DC was able to synthesize ZnONPs because the presence of secondary metabolites (reducing enzymes and capping agents) causes Zn $(NO_3)_2$ changed from (oxidation state +2 to 0). The formation of DC-ZnONPs was indicated by the DC root extract's colour changing from purple to yellow (Figure 1a). While the gold precursor in this study was HAuCl4 (1 mM), and DC root extract was used as a reducing and stabilizing agent. We discovered that the phytochemical substances in the DC aqueous root extract, as well as secondary metabolites, are involved in the formation of nanoparticles and convert $AuCl_4$ to Au (oxidation state +3 to 0). The formation of AuNPs was indicated by the DC root extract's colour changing from brown to ruby red (Figure 1).

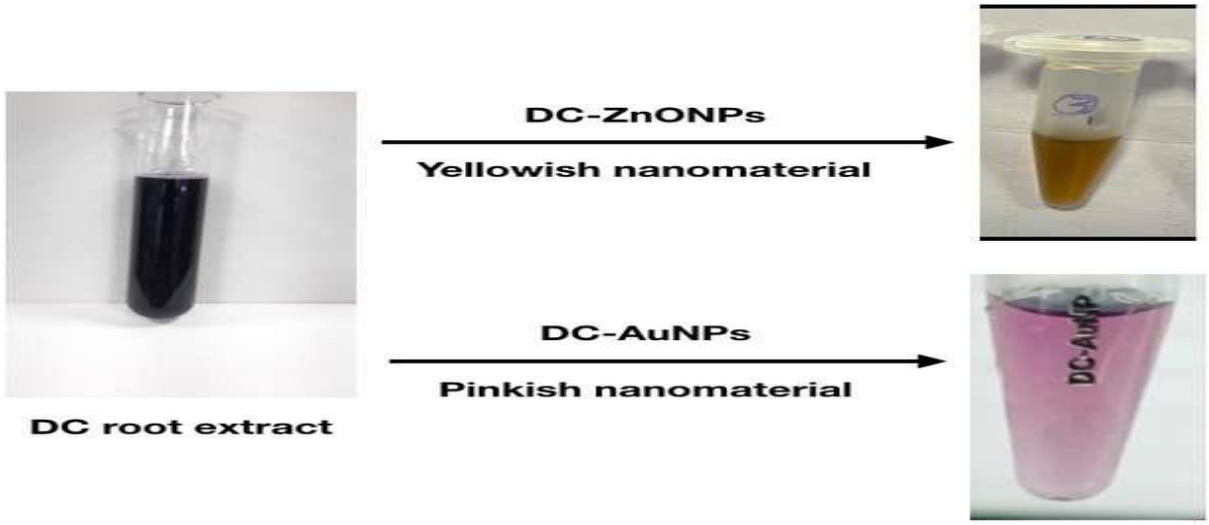

Figure 1: Formation of DC-ZnONPs and DC-AuNPs

The surface plasmon resonance (SPR) band of the DC-ZnONPs is shown by the absorption peak that was observed at 342 nm. The presence of a distinctive absorption peak of DC-ZnONPs at 342 nm confirmed the synthesis of DC-ZnONPs. It can be identified by a color shift from purple to yellow. U.V. vis spectroscopy confirms the production of DC-ZnONPs (Figure 2) and DC-AuNPs (Figure 2). A distinct absorption peak of DC-AuNPs at 526 nm confirmed the synthesis of DC-AuNPs. It can be identified by a colour shift from light brown to ruby red (DC-AuNPs).

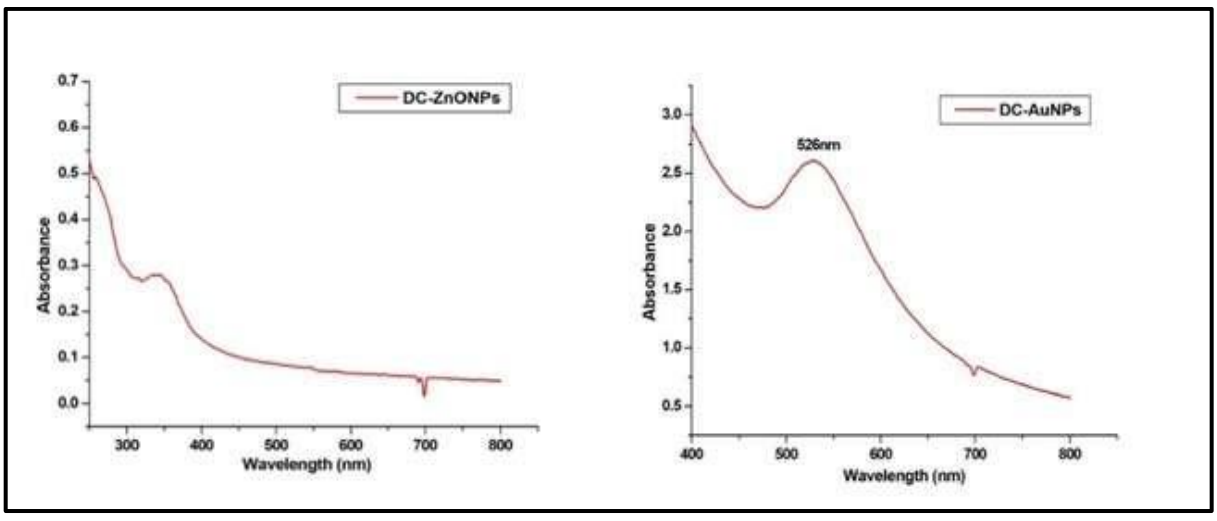

Figure 2: UV vis spectrum of synthesized DC-ZnONPs and DC-AuNPs.

Using DLS, the average particle size and distribution profile of the synthesized nanoparticles were analyzed. With median particle size of 66 nm and polydispersity index (PDI) of 0.041, DC-ZnONPs showed homogeneous size distribution, as shown in Figure 3A. In general, a zeta value of ± 20 mV is needed for nanoparticle colloidal stability. With zeta potentials of -13 mV respectively, the synthesized DC-ZnONPs exhibit exceptional particle stability (Figure 3B). Through DLS analysis, the synthesised nanoparticles average particle size and distribution profile were ascertained. With a median particle size of 59 nm, respectively, and a polydispersity index (PDI) of 0.041, DC-AuNPs showed homogeneous size distributions, as shown in Figure 3C. Figure 3D demonstrates the zeta potential of the AuNPs. Generally, nanoparticle colloidal stability implies a zeta value of ±20 mV. With zeta potential of -17 mV, respectively, the synthesized DC-AuNPs exhibit phenomenal particle stability. During storage at room temperature, no clumping or agglomeration was seen in the aqueous solution of DC-ZnONPs and DC-AuNPs. This could be related to the electrostatic repulsive interactions among the nanoparticles, which hindered them from approaching each other.

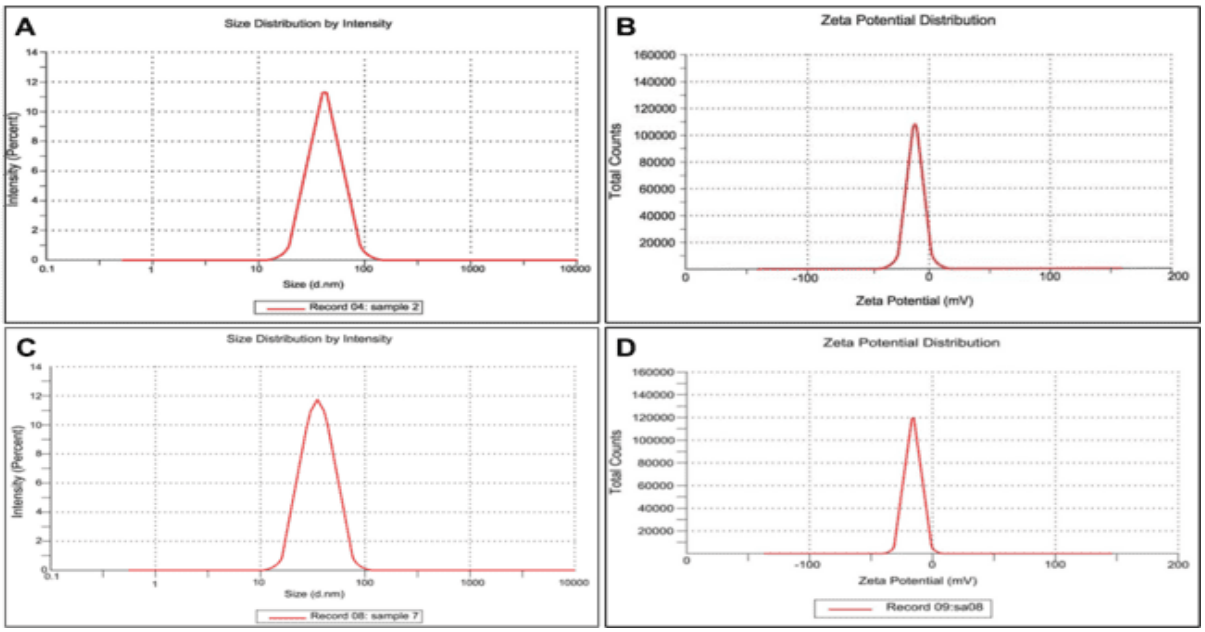

Figure 3: Dynamic light scattering measurements for DC-ZnONPs and DC-AuNPs are shown in (A) and (C), respectively. The zeta potential results for DC-ZnONPs and DC-AuNPs are presented in (B) and (D), respectively.

According to TEM micrographs (Figure 4A), the particles are equally dispersed and have a spherical shape with a negligible aggregation. The average size of the DC-ZnONPs produced by TEM was 25 ± 2 nm, respectively. Compared to the average size determined by DLS, this was significantly smaller. While DC-AuNPs were spherical and evenly distributed, without significant aggregation. The average diameter of the DC-AuNPs generated by TEM was 23 ± 2 nm, respectively. Compared to the average size determined by DLS, this was significantly smaller (Figure 4B). TEM measures the exact diameter of the particles as they are observed in the dry state (hydrated state), in contrast to the hydrodynamic diameter given by the DLS technique. Accordingly, under hydrated conditions, the solvent effect causes particles to have a larger hydrodynamic volume.

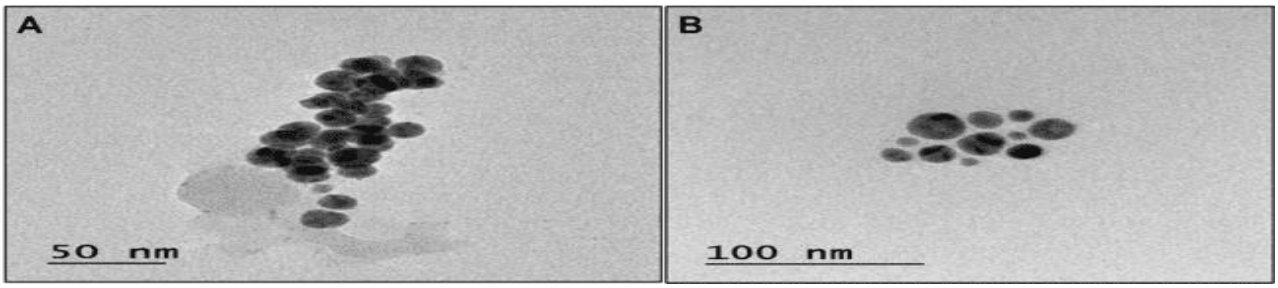

Figure 4: Transmission electron microscopy of (A) DC-ZnONPs and (B) DC-AuNPs

The FTIR spectra of DC-ZnONPs showed a peak at 3393.16 cm-¹, respectively, that was attributed to N-H stretching (aliphatic primary amine) groups as well as alcohol group. Because of the C=C stretching (alkene) in the synthesized NPs, the peak was seen at 1639.31 cm− ¹ (Figure 5B). The peak at 1231.08 is the C-O bond in an ethanoate. The C-O stretching vibration, which is dependent on the strength of the carbonyl group showed the peak at 1157.77 cm-¹. Additionally, at 1067.92 cm-¹, ether as well as aliphatic or C–O stretching vibrations were detected. On the other hand, the spectra of DC-AuNPs (Figure 5C) showed peak at 3394.48 cm-¹, respectively, that were attributed to N-H stretching (aliphatic primary amine) groups as well as alcohol group. The peak at 2923.72 cm-¹ is consistent of C-H stretching. Because of the C=C stretching (alkene) in the synthesized NPs, the peak was seen at 1634.50 cm− ¹. The peak at 1229.50 cm-¹ is the C-O bond in an ethanoate. The C-O stretching vibration, which is dependent on the strength of the carbonyl group showed the peak at 1157.77 cm-¹. Furthermore, at 1068.31 cm-¹, ether as well as aliphatic or C–O stretching vibrations were detected. The peak located at 770.49 cm−1 in the synthesized AuNPs demonstrated a significant appearance of an aromatic mono-substituted (C-C).

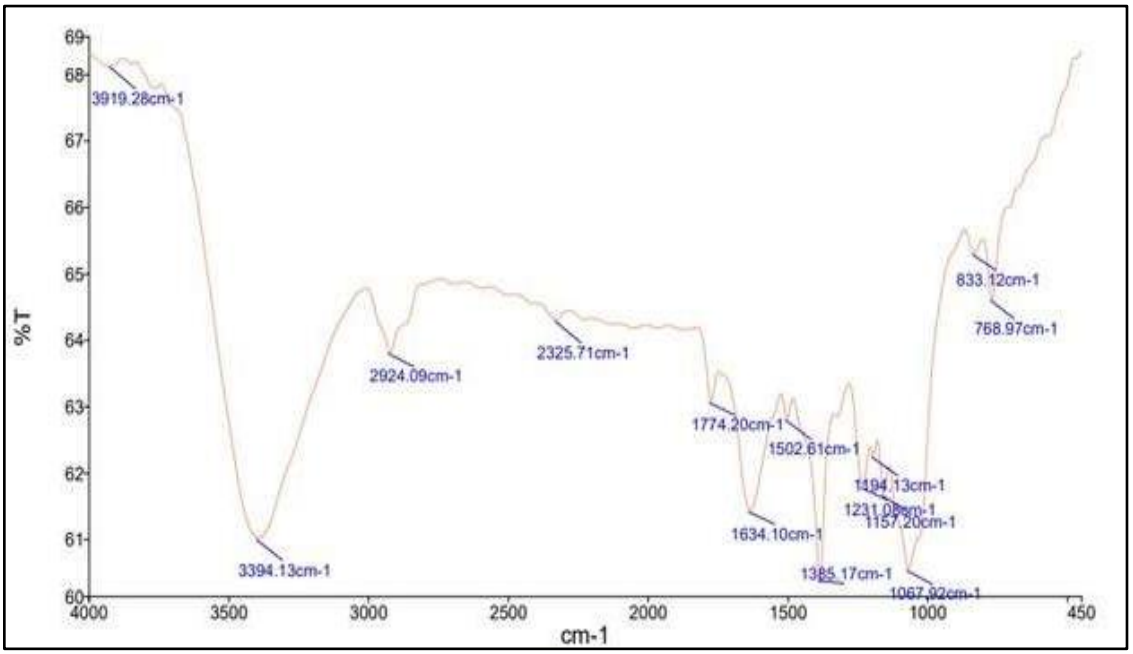

Figure 5: FTIR spectra of (A) DC root extract.

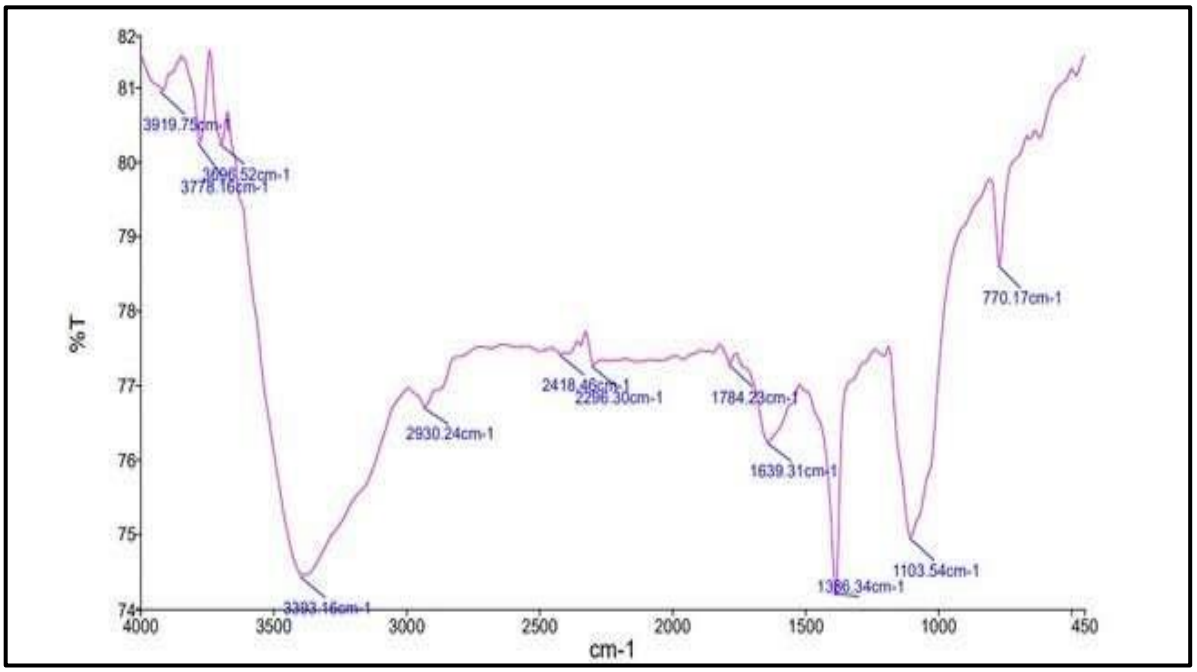

Figure 5: FTIR spectra of (B) DC-ZnONPs.

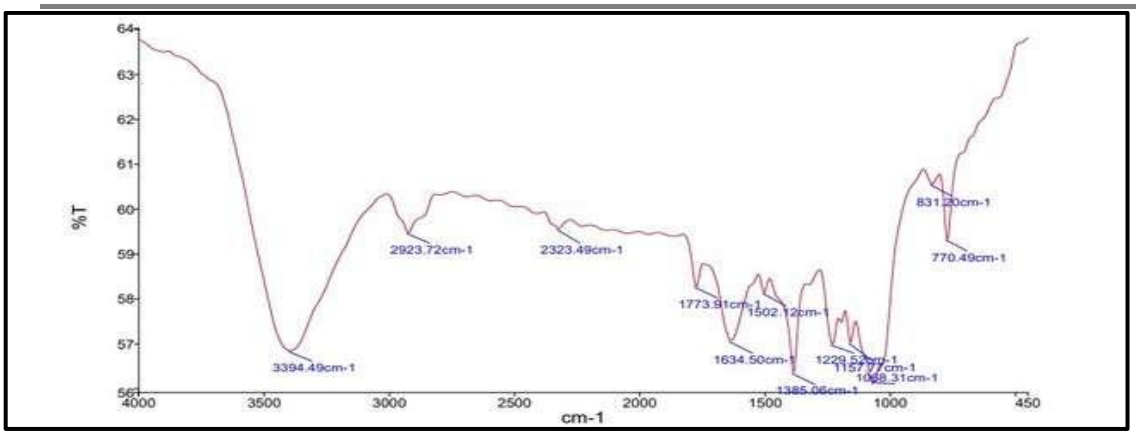

Figure 5: FTIR spectra of (C) DC-AuNPs

Zone of inhibitions

Synthesized nanoparticles were analyzed against gram-negative (*Escherichia coli*, and *Pseudomonas aeruginosa*) and gram-positive (*Staphylococcus aureus*, and *Bacillus subtilis*) to check their antimicrobial efficacy. The chosen strains for the study encompass a range of bacterial machinery types that exhibit many virulence factors, along with their evident toxicity and significant human prevalence. According to the experiment, the nanomaterials may spread throughout the agar and stop the growth of bacteria. The antibacterial activity was evaluated by introducing synthesized DC-ZnONPs, DC-AuNPs, DC Root extract, standard drug levofloxacin, and negative control (PBS) into wells on MH agar plates. The experiments were performed in triplicate, with the agar plates incubated overnight at 37 °C. The size of the inhibition zone was measured (Figure 6). Subsequent observations revealed that both DC-ZnONPs, DC-AuNPs**,** and DC Root extract diffused through the agar medium, effectively inhibiting bacterial growth.

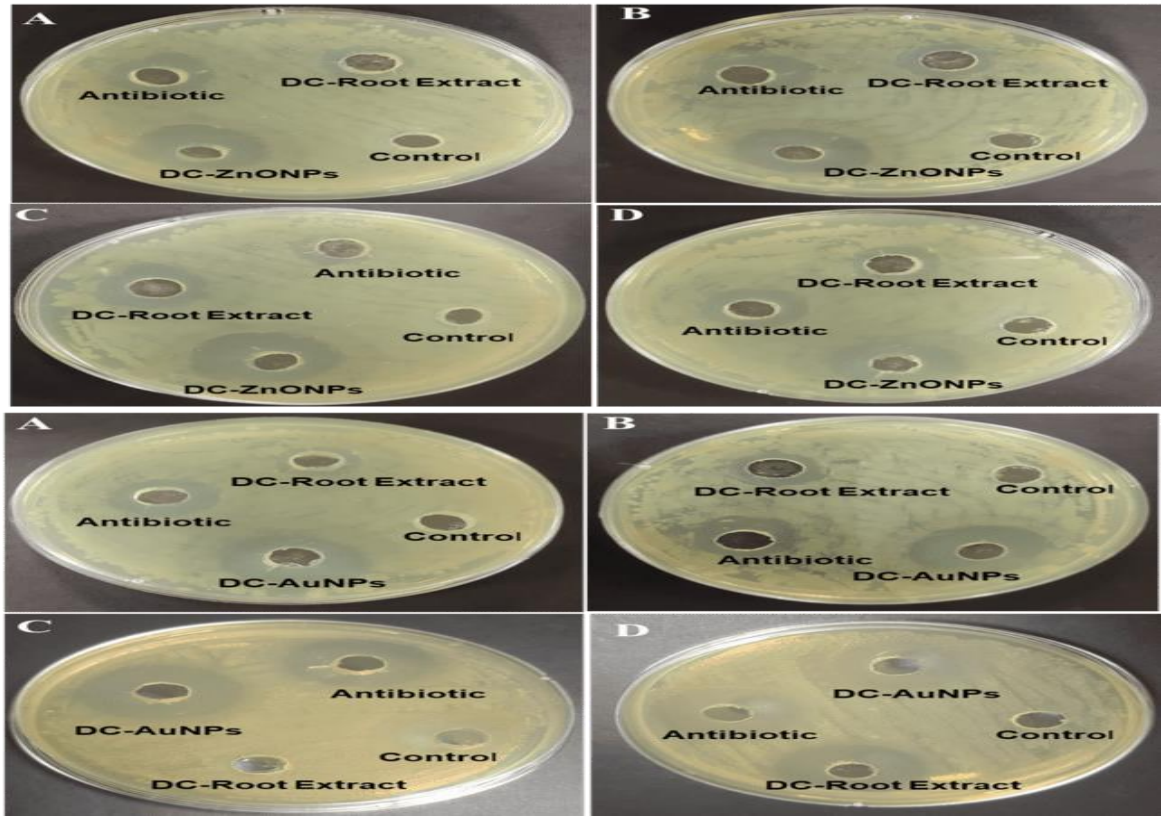

Figure 6: Antibacterial activity of synthesized DC-ZnONPs, DC-AuNPs, DC-Root Extract, and standard antibiotic (levofloxacin) was determined using agar well diffusion method (A) *Bacillus subtilis*, (B) Escherichia coli, (C) Pseudomonas aeruginosa, and (D) Staphylococcus aureus Minimum inhibitory concentration of DC-ZnONPs and DC-AuNPs

The minimum inhibitory concentrations (MICs) were generated from DC-ZnOPs, DC-AuNPs, and DC root extract against the tested bacterial strains. In 96-well microtiter plates, nanoparticles were diluted gradually using Tryptic Soy Broth (TSB) medium to provide an array of concentrations (1–100 µg/mL of DC-ZnOPs and 0.1–120 µg/mL of DC-AuNPs and 0.1-100 µg/mL). An aliquot (100 µL) of standard suspensions of the tested bacterial strain was added to each well. An aliquot (100 µL) of standard suspensions of the tested bacterial strain was added to each well. Following a 24-hour incubation period at 37°C and the viability counting of bacterial cells in each well, the lowest dosages of DC root extract, DC-ZnONPs, and DC-AuNPs that suppressed the growth of bacteria were found to be the MICs (Rizvi et al., 2011). The MIC_{50} of DC-ZnONPs result indicates that at doses of MIC_{50} 6.15 µg/mL, 6.4 µg/mL, 7.31 µg/mL and 5.2 µg/mL of DC-ZnONPs, 24.30 µg/mL, 30.17 µg/mL, 28.91 µg/mL, and 19.04 µg/mL of DC root extract, and 11.99 µg/mL, 15.09 µg/mL, 20.92 µg/mL, and 14.34 µg/mL Levofloxacin (standard drug) showed effective inhibition against the *Escherichia coli, Pseudomonas aeruginosa, Staphylococcus aureus,* and *Bacillus subtilis* respectively. Hence, when compared to the control group and standard drug used, DC-ZnONPs showed the best MIC_{50} against gram-positive and gram-negative bacterial strains (Figure 7). While the MIC_{50} of DC-AuNPs that inhibited bacterial growth by 50% was recognized as the $MIC_{50.}$ At MIC_{50} doses of 9.3, 5.4, 5.95 and 7.57 µg/mL DC-AuNPs, 32.42, 37.41, 20.75, and 24.49 µg/mL of DC root extract 25.96, 17.11, 15.83, and 12.18 µg/mL Levofloxacin showed inhibition against the *Escherichia coli, Pseudomonas aeruginosa*, *Staphylococcus aureus* and *Bacillus subtilis.* (Figure 8). Electron microscopy was used to detect the irregularly shaped nanoparticles, which ranged in size from 10 to 20 nm. When tested against various bacterial strains, the synthesised nanoparticle possessed good MIC_{50} values. Consequently, DC-AuNPs demonstrated the best MIC_{50} against *E coli, P. aeruginosa, S. aureus and B. subtilis* (9.3, 5.4, 5.95 and 7.57 µg/mL).

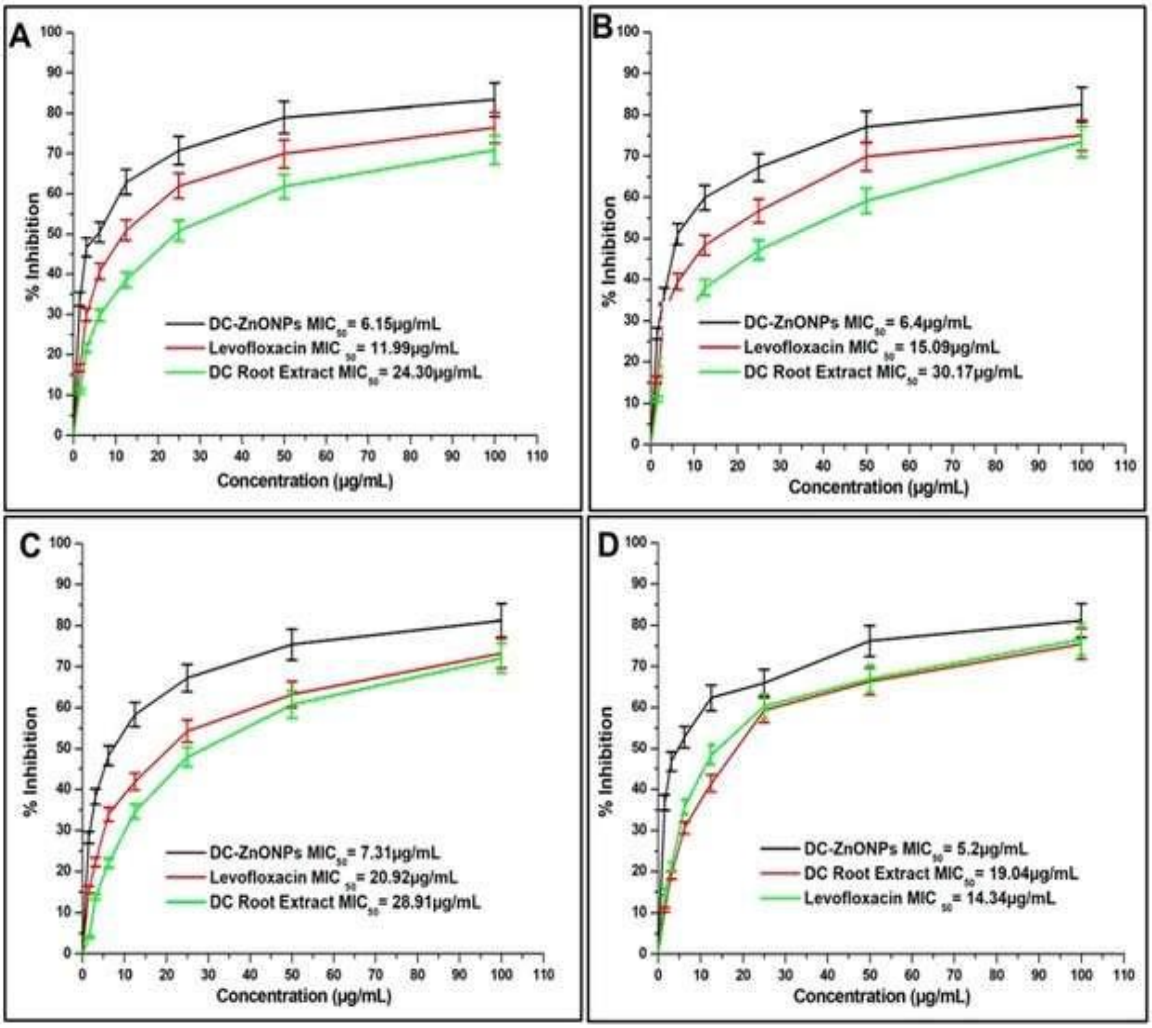

Figure 7: Minimum inhibitory concentration (MIC) of DC-ZnONPs, DC Root Extract, and Levofloxacin against A) *Escherichia coli* B) *Pseudomonas aeruginosa* C) *Staphylococcus aureus*, and D) *Bacillus subtilis*. The data represent the mean ± standard error of three independent experiments.

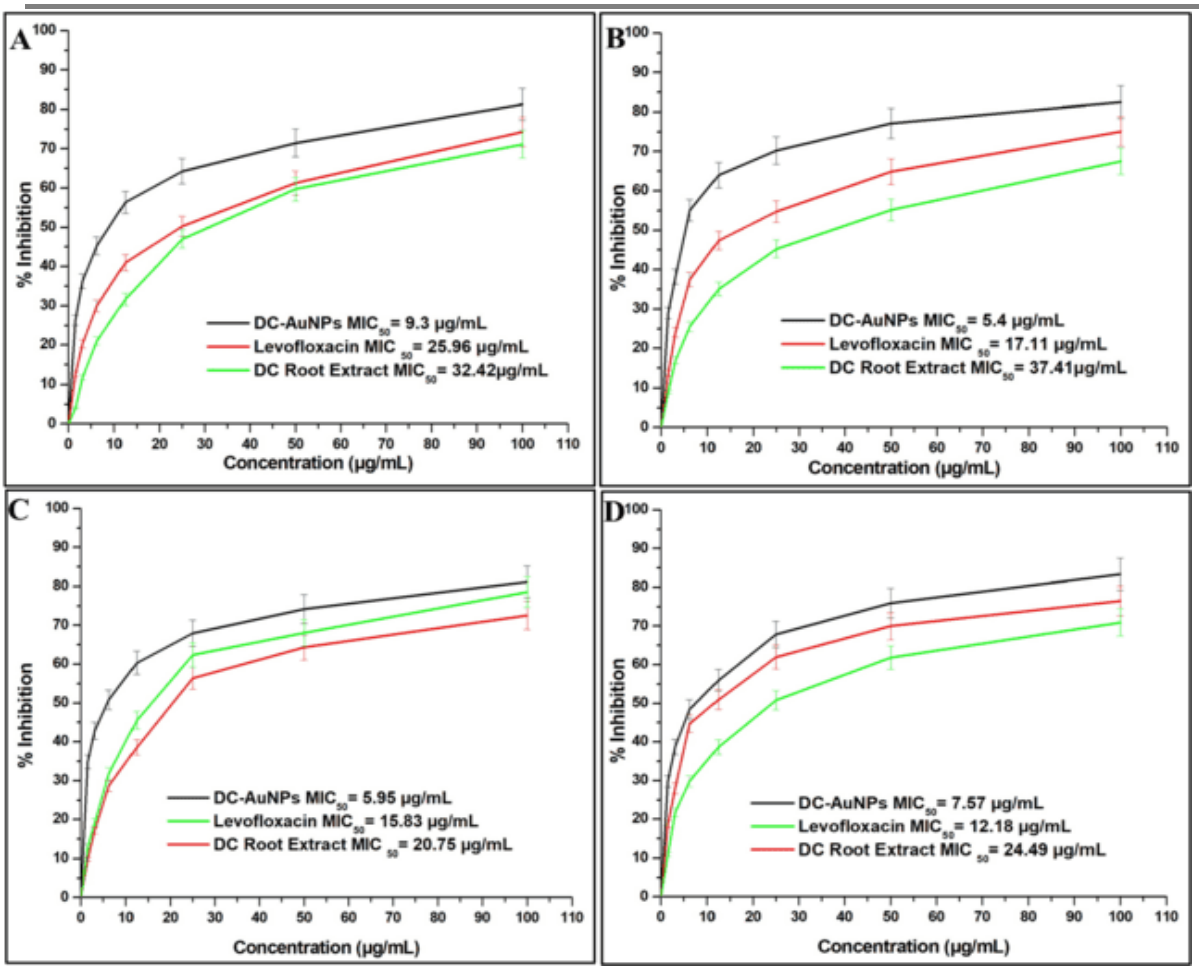

Figure 8: Minimum inhibitory concentration (MIC) of DC-AuNPs, DC Root Extract, and Levofloxacin against A) *Escherichia coli* B) *Pseudomonas aeruginosa* C) *Staphylococcus aureus*, and D) *Bacillus subtilis*. The data represent the mean ± standard error of three independent experiments.

Estimation of IC_{50} value of DC-ZnONPs and DC-AuNPs

The potential of DC-ZnONPs was found to be significantly greater than DC root extract against A549 cells while it did not show any cytotoxic effect against primary osteoblast cells**.** The viability of A549 cells declined rapidly within the concentration range of 1.56 to 100 µg/mL, ultimately resulting in an IC_{50} value of 12.40 µg/mL, 29.62 µg/mL, and 20.21 µg/mL for DC-ZnONPs, DC root extract and 5-Fu respectively (Figure 9A).

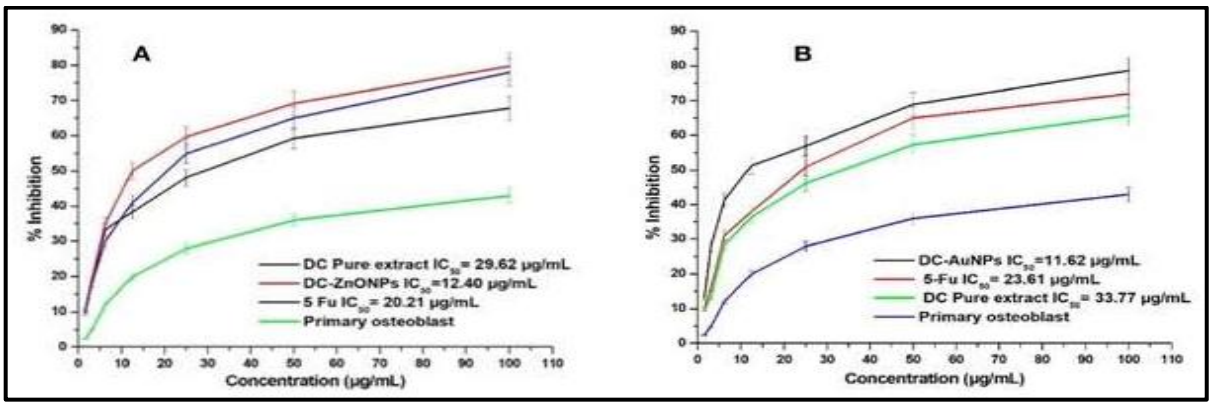

Figure 9: IC_{50} value of DC-ZnONPs and DC-AuNPs against cancer cell lines

While the average half-lives of DC root extract, DC-AuNPs, and 5-FU in A549 cells were found to be 33.77 µg/mL, 11.62 µg/mL, and 23.61 µg/mL, respectively. DC root extract and DC-AuNPs showed less cytotoxic effect on primary osteoblasts, even with increased acceptable biological limits (1 µg/mL). The IC_{50} value

recorded with the treatment of DC-AuNPs was 11.62 µg/mL, as demonstrated by the MTT results, while the IC_{50} of the DC root extract was 33.77 µg/mL. Compared to DC-AuNPs, DC root extract showed a higher IC_{50} value in A549 cell lines. DC-AuNPs coated with phytochemicals worked better than the pure compounds. Moreover, research on primary osteoblasts showed that at concentrations of 11.62-33.77 µg/mL or above, neither DC-AuNPs nor DC root extract significantly reduced cell death (Figure 9B).

Cytomorphological analysis

The morphological changes in A549 were studied by incubating DC root extract, DC-ZnONPs (Figure 9A–D), DC-AuNPs (Figure 10A–D), and 5-Fu at IC_{50} concentrations under a phase contrast inverted microscope. The untreated (or control) cells were found to be unaffected with no change in native morphology after 24 hours of incubation. Many observable morphological alterations (circular morphologies), cell clumping, loss of membrane integrity, cytoplasm condensation, and inhibition of cell development were seen in treated A549 cells (Figure 9&10A–D).

Analysis of changes in nuclear morphology

We performed experiments in triplicate, ensuring the reproducibility of our findings. Our research into how DC-ZnONPs and DC-AuNPs are internalized and subsequently interact with nuclear components, utilizing DAPI staining techniques, demonstrated significant apoptotic effects in A549 cells. These effects were evidenced by notable alterations in nuclear morphology, including the condensation of chromatin, which are likely facilitated by enhanced permeability of the cell membrane (Figure 9 E–H). While the ability of DC-AuNPs to interact with malignant cells was investigated using DAPI, a fluorescent dye (Figure 10E–H). Increased cell membrane penetrability may have contributed to the severe apoptotic effects seen in A549 cells. Compared to untreated cells, these effects were shown by condensed chromatin and dark blue fluorescent integrated nuclei.

Estimation of a generation of Reactive Oxygen Species (ROS)

The extent of intracellular ROS generation in the A549 cells upon interaction with DC-ZnONPs, DC-AuNPs, DC root extract, and 5-Fu at IC_{50} concentrations was estimated by utilizing 5 (6)- carboxy-2',7' 7'-dichlorodihydrofluorescein diacetate (DCFHDA) as an oxidation-sensitive fluorogenic marker of ROS in the viable cells. The intensity of fluorescence was found to be directly proportional to the generation of ROS in the cells. The given analysis verified that DC-ZnONPs and DC-AuNPs treated with A549 cells were found to produce greater intensities of fluorescence for their controls (Figure 10–I). Similarly, Figure 10 I–L illustrates the comparable pattern in ROS quantification using the DCFHDA dye assay. On the other hand, there is no apparent distinction in the normal osteoblast cell in the influence of DC-ZnOPs and DC-AuNPs.

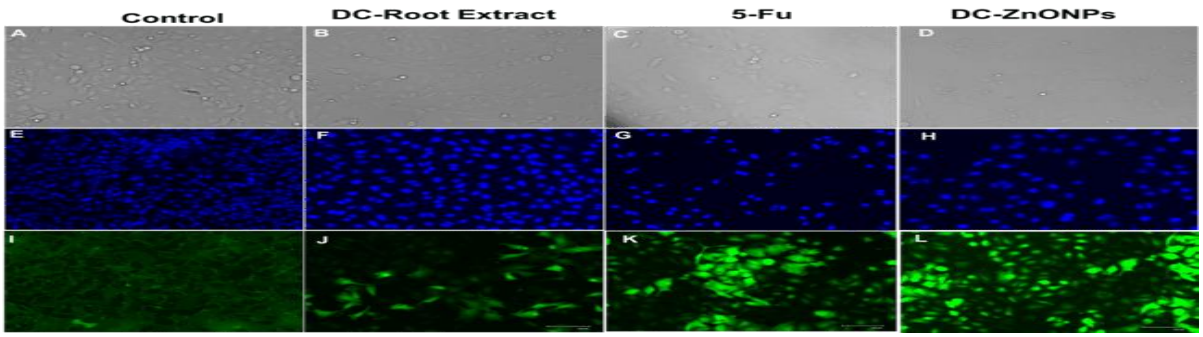

Figure 10: Cytomorphological images of A549 cells treated with IC_{50} of DC-ZnONPs, DC-Root Extract, and 5-Fu (A–D). A549 cells have been stained with the fluorescent nuclear dye DAPI. Approximately 50% of DAPI-stained treated or untreated A549 cells with DC-ZnONPs, DC-Root Extract, and 5-Fu at the IC_{50}, were assessed in (E–H). Qualitative evaluation of ROS in H2DCFDA-stained A549 cell treated at IC_{50} concentration of DC-ZnONPs, DC-Root Extract, and 5-Fu for 24 h analyzed by fluorescence microscopy shown in (I-L). The images shown are representative of three independent experiments performed in triplicates.

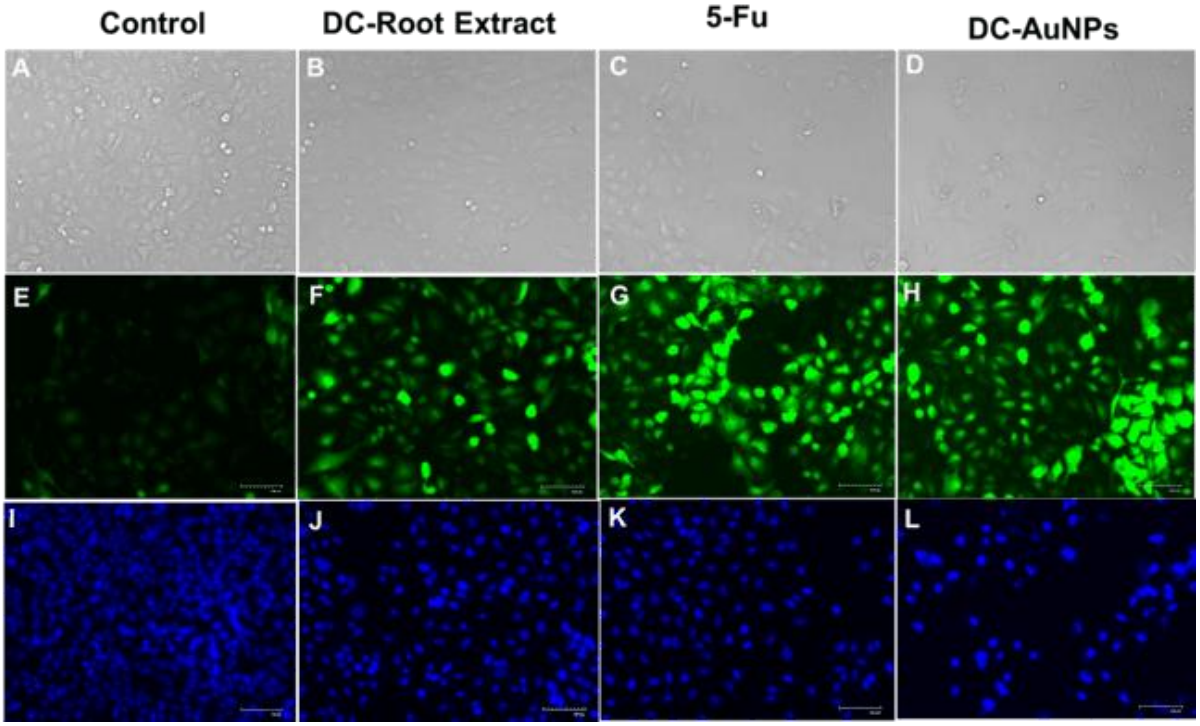

Figure 11: Cytomorphological images of A549 cells treated with IC_{50} of DC-AuNPs, DC-Root Extract, and 5-Fu (A–D). A549 cells have been stained with the fluorescent nuclear dye DAPI. Approximately 50% of DAPI-stained treated or untreated A549 cells with DC-AuNPs, DC-Root Extract, and 5-Fu at the IC_{50}, were assessed in (E–H). Qualitative evaluation of ROS in H2DCFDA-stained A549 cell treated at IC_{50} concentration of DC-AuNPs, DC-Root Extract, and 5-Fu for 24 h analyzed by fluorescence microscopy shown in (I–L). The images shown are representative of three independent experiments performed in triplicates.

DISCUSSIONS

The remarkable achievements of diverse nanomaterials in antimicrobial, anti-inflammatory, and anticancer research lead to its use as an alternative approach for the management of bacterial infections and cancer [27]. Based on data supplied by 87 countries in 2020, new World Health Organization (WHO) research finds significant levels of resistance in bacteria that cause potentially fatal bloodstream infections. It also shows that some bacteria that cause common infections in the community are becoming more resistant to treatment [28]. On the other hand, 20 million new instances of cancer and 9.7 million deaths from the disease are predicted for 2022. 53.5 million people were predicted to still be alive five years after receiving a cancer diagnosis. One in five people will have cancer at some point in their lives; one in nine men and one in twelve women will pass away from the illness [29]. Therefore, there is a need for novel nanomaterials to quench the bacterial infection and cancer. The present study designed a novel nanomaterial by using the root extract of Daucus carota (DC) to synthesize ZnONPs and AuNPs [Figure 1]. The phytochemicals present in Daucus carota are phenolics, carotenoids, polyacetylenes, and ascorbic acid, which are known to reduce cancer, and cardiovascular diseases due to their antioxidant, anti-inflammatory, plasma lipid modification, and anti-tumor properties [29]. The characterisation of DC-ZnONPs DC-AuNPs has been carried out through various physicochemical analyses using UV–visible spectroscopy [Figure 2], FTIR spectroscopy [Figure 5A–C], DLS, zeta potential [Figure 3], and TEM microscopy. Optical absorption spectroscopy is a commonly used technique to evaluate the optical characteristics of nanosized particles. When nanoparticle sizes are determined using DLS, the hydrodynamic diameter of the particles is estimated, [30], and the size distribution of DC-ZnONPs and DC-AuNPs is observed as homogeneous. The concentration, distribution, exposure or shielding of charged moieties, ionization, and adsorption of DC-ZnONPs and DC-AuNPs can all be readily obtained using zeta potential. Zeta potentials of -13 mV verify that DC with ZnONPs and DC with AuNPs are conjugated. TEM was used to characterize the shape and size of DC-ZnONPs and DC-AuNPs that were synthesized using a root extract of DC [Figure 4]. The TEM images clearly showed that the synthesized nanomaterials were almost spherical,

with the average diameter of nanoparticles ranging from 25 ± 2 nm approximately. To determine the growth prevention effects of DC-ZnONPs and DC-AuNPs applied to the culture medium of *Escherichia coli, Pseudomonas aeruginosa, Staphylococcus aureus, and Bacillus subtilis,* we observed that both the nanomaterials inhibit the growth of both gram-negative and gram-positive bacteria and that the antibacterial efficiency of DC-ZnONPs and DC-AuNPs is higher than standard drug levofloxacin [Figure 6]. Similarly, it showed agreeable MIC₅0 which has effective antibacterial effects [Figure 7 & 8]. Likewise, the in-vitro cytotoxic effect of DC-ZnONPs and DC-AuNPs was evaluated on the A549 lung cancer cell line at different concentrations (3.125 to 100 µg/mL) by using MTT assay [Figure 9], whereas primary osteoblasts cells were taken as control. The cytotoxic effect of both the nanomaterials on cell lines was dose-dependent. In A549 cells, with an increase in the concentration of nanomaterials, the anticancerous effect also increases. When treated with DC-ZnONPs and DC-AuNPs separately, A549 cells, and primary osteoblast cells showed enhanced permeability and an apoptotic impact. This led to condensed chromatin and a deep blue fluorescence condensed nucleus in the A549 cells (Figure 10 & 11) compared to their control cells. The nucleus condensation is the most notable and specific indicator of the cytotoxic effect brought on by stress. Similar trend was also observed during the ROS measurement of A549 cells under the treatment of the nanoparticle. No significant ROS generation was detected in A549 cells with DC-ZnONPs and DC-AuNPs treatment compared to the control (Figure 10 & 11), suggesting that DC-ZnONPs and DC-AuNPs have significant biological effects over the production of oxidative stress.

CONCLUSION

Nanomaterials have been widely utilized, particularly because of their large surface area. It gained significant attention due to their large surface area and versatile applications, particularly as active catalysts and support materials in important organic transformations for industrial processes. In this research, the green synthesis of novel nanoparticles was successfully developed, demonstrating stability and potential as both an antibacterial and anticancer agent. The antibacterial studies, conducted on both gram-positive and gram-negative bacterial strains, highlighted the potent efficacy of nanomaterials in combating bacterial infections. Furthermore, the anticancer studies revealed that they possess the ability to inhibit lung cancer cell proliferation, positioning them as promising agents for future therapeutic applications in oncology and infectious disease management.

Author Contributions:

MI: Investigation, Writing-original draft, Conceptualization, Methodology, Resources, Supervision, Validation, Writing–review and editing.

SV: Formal Analysis, Writing-review and editing

SV: Formal Analysis, Investigation, Methodology, Writing-review and editing

Funding

The author(s) declare that no financial support was received for this article's research, authorship, and/or publication.

Data Availability Statement

The data that support the findings of this study are available upon reasonable request.

ACKNOWLEDGMENTS:

The authors express their heartfelt gratitude to JKKMMRF'S Annai JKK Sampoorani Ammal College of Pharmacy, Namakkal, Tamil Nadu for providing the necessary infrastructure.

Conflicts of Interest

Nil

REFERENCES

1. Ahmad, N.M.; Mohamed, A.H.; Hasan, N.; Zainal-Abidin, N.; Nawahwi, M.Z.; Azzeme, A.M. Effect of Optimisation Variable and the Role of Plant Extract in the Synthesis of Nanoparticles Using Plant-Mediated Synthesis Approaches. Inorg. Chem. Commun. **2024**, 161, 111839.
2. Beheshtkhoo, N.; Kouhbanani, M.A.J.; Savardashtaki, A.; Amani, A.M.; Taghizadeh, S. Green Synthesis of Iron Oxide Nanoparticles by Aqueous Leaf Extract of Daphne Mezereum as a Novel Dye Removing Material. Appl. Phys. A **2018**, 124, 1–7.
3. Nayal, R.; Mejjo, D.; Abajy, M.Y. Anti Inflammatory Properties and Safety of Green Synthesized Metal and Metal Oxidenanoparticles: A Review Article. Eur. J. Med. Chem. Reports **2024**, 100169.
4. Sánchez-López, E.; Gomes, D.; Esteruelas, G.; Bonilla, L.; Lopez-Machado, A.L.; Galindo, R.; Cano, A.; Espina, M.; Ettcheto, M.; Camins, A.; et al. Metal-Based Nanoparticles as Antimicrobial Agents: An Overview. Nanomaterials **2020**, 10, 292, doi:10.3390/nano10020292.
5. Mishra, P.; Faruqui, T.; Akhtar, S.; Nadeem, I.; Khan, I.; Wabaidur, S.M.; Kazi, M.; Rahim, M.; Rafi, Z.; Khan, S. Antiproliferative Activity of Gold and Silver Nanoparticles Fabricated Using Bark Extract of Murraya Koenigii. J. Drug Deliv. Sci. Technol. **2023**, 89, 105014.
6. Elumalai, K.; Velmurugan, S. Green Synthesis, Characterization and Antimicrobial Activities of Zinc Oxide Nanoparticles from the Leaf Extract of Azadirachta Indica (L.). Appl. Surf. Sci. **2015**, 345, 329–336.
7. Kumar, D.; Saini, N.; Jain, N.; Sareen, R.; Pandit, V. Gold Nanoparticles: An Era in Bionanotechnology. Expert Opin. Drug Deliv. **2013**, 10, 397–409.
8. Anbukkarasi, V.; Srinivasan, R.; Elangovan, N. Antimicrobial Activity of Green Synthesized Zinc Oxide Nanoparticles from Emblica Officinalis. Int. J. Pharm. Sci. Rev. Res **2015**, 33, 110–115.
9. Santhoshkumar, J.; Kumar, S.V.; Rajeshkumar, S. Synthesis of Zinc Oxide Nanoparticles Using Plant Leaf Extract against Urinary Tract Infection Pathogen. Resour. Technol. **2017**, 3, 459–465.
10. Luque, P.A.; Nava, O.; Romo-Cardenas, G.; Nieto-Hipolito, J.I.; Vilchis-Nestor, A.R.; Valdez, K.; de Dios Sanchez-Lopez, J.; Murrieta-Rico, F.N. Facile Zinc Oxide Nanoparticle Green Synthesis Using Citrus Reticulata Extract for Use in Optoelectronic Sensors. IEEE Sens. J. **2020**, 21, 11275–11282.
11. Sirelkhatim, A.; Mahmud, S.; Seeni, A.; Kaus, N.H.M.; Ann, L.C.; Bakhori, S.K.M.; Hasan, H.; Mohamad, D. Review on Zinc Oxide Nanoparticles: Antibacterial Activity and Toxicity Mechanism. Nano-micro Lett. **2015**, 7, 219–242.
12. Tian, F.; Bonnier, F.; Casey, A.; Shanahan, A.E.; Byrne, H.J. Surface Enhanced Raman Scattering with Gold Nanoparticles: Effect of Particle Shape. Anal. Methods **2014**, 6, 9116–9123.
13. Sani, A.; Cao, C.; Cui, D. Toxicity of Gold Nanoparticles (AuNPs): A Review. Biochem. Biophys. reports **2021**, 26, 100991.
14. Iravani, S. Green Synthesis of Metal Nanoparticles Using Plants. Green Chem. **2011**, 13, 2638–2650.
15. Nadagouda, M.N.; Varma, R.S. Green Synthesis of Silver and Palladium Nanoparticles at Room Temperature Using Coffee and Tea Extract. Green Chem. **2008**, 10, 859–862.
16. Al-darwesh, M.Y.; Ibrahim, S.S.; Mohammed, M.A. A Review on Plant Extract Mediated Green Synthesis of Zinc Oxide Nanoparticles and Their Biomedical Applications. Results Chem. **2024**, 7, 101368.
17. Farhana, A.; Alsrhani, A.; Rasheed, N.; Rasheed, Z. Gold Nanoparticles Attenuate the Interferon-γ Induced SOCS1 Expression and Activation of NF-KB P65/50 Activity via Modulation of MicroRNA-155-5p in Triple-Negative Breast Cancer Cells. Front. Immunol. **2023**, 14, 1228458.
18. Agcam, E.; Akyıldız, A.; Kamat, S.; Balasubramaniam, V.M. Bioactive Compounds Extraction from the Black Carrot Pomace with Assistance of High Pressure Processing: An Optimization Study. Waste and Biomass Valorization **2021**, 1–19.
19. Smeriglio, A.; Denaro, M.; Barreca, D.; D'Angelo, V.; Germanò, M.P.; Trombetta, D. Polyphenolic Profile and Biological Activities of Black Carrot Crude Extract (Daucus Carota L. Ssp. Sativus Var. Atrorubens Alef.). Fitoterapia **2018**, 124, 49–57.
20. Soares, G.R.; de Moura, C.F.G.; Silva, M.J.D.; Vilegas, W.; Santamarina, A.B.; Pisani, L.P.; Estadella, D.; Ribeiro, D.A. Protective Effects of Purple Carrot Extract (Daucus Carota) against Rat Tongue Carcinogenesis Induced by 4-Nitroquinoline 1-Oxide. Med. Oncol. **2018**, 35, 1–14.
21. Paprocka, P.; Durnaś, B.; Mańkowska, A.; Król, G.; Wollny, T.; Bucki, R. Pseudomonas Aeruginosa

Infections in Cancer Patients. Pathogens **2022**, 11, 679.

22. Alshahrani, M.Y.; Rafi, Z.; Alabdallah, N.M.; Shoaib, A.; Ahmad, I.; Asiri, M.; Zaman, G.S.; Wahab, S.; Saeed, M.; Khan, S. A Comparative Antibacterial, Antioxidant, and Antineoplastic Potential of Rauwolfia Serpentina (L.) Leaf Extract with Its Biologically Synthesized Gold Nanoparticles (r-Aunps). Plants **2021**, 10, 2278.
23. Khan, S.; Rafi, Z.; Baker, A.; Shoaib, A.; Alkhathami, A.G.; Asiri, M.; Alshahrani, M.Y.; Ahmad, I.; Alraey, Y.; Hakamy, A. Phytochemical Screening, Nutritional Value, Anti-Diabetic, Anti-Cancer, and Anti-Bacterial Assessment of Aqueous Extract from Abelmoschus Esculentus Pods. Processes **2022**, 10, 183.
24. Khan, S.; Haseeb, M.; Baig, M.H.; Bagga, P.S.; Siddiqui, H.H.; Kamal, M.A.; Khan, M.S. Improved Efficiency and Stability of Secnidazole–An Ideal Delivery System. Saudi J. Biol. Sci. **2015**, 22, 42–49.
25. Rizvi, S.M.D.; Zeeshan, M.; Khan, S.; Biswas, D.; Al-Sagair, O.A.; Arif, J.M. Evaluation and Distribution of Antibacterial Potential in the Aerial Parts of Wild Tridax Procumbens. J. Chem. Pharm. Res. **2011**, 3, 80–87.
26. Iram, S.; Zahera, M.; Khan, S.; Khan, I.; Syed, A.; Ansary, A.A.; Ameen, F.; Shair, O.H.M.; Khan, M.S. Gold Nanoconjugates Reinforce the Potency of Conjugated Cisplatin and Doxorubicin. Colloids Surfaces B Biointerfaces **2017**, 160, 254–264.
27. Hembram, K.C.; Kumar, R.; Kandha, L.; Parhi, P.K.; Kundu, C.N.; Bindhani, B.K. Therapeutic Prospective of Plant-Induced Silver Nanoparticles: Application as Antimicrobial and Anticancer Agent. Artif. cells, nanomedicine, Biotechnol. **2018**, 46, 38–51.
28. Prestinaci, F.; Pezzotti, P.; Pantosti, A. Antimicrobial Resistance: A Global Multifaceted Phenomenon. Pathog. Glob. Health **2015**, 109, 309–318.
29. Lu, Y.; Mei, N.; Ying, Y.; Wang, D.; Li, X.; Zhao, Y.; Zhu, Y.; Shen, S.; Yin, B. Bacteria-Based Nanoprobes for Cancer Therapy. Int. J. Nanomedicine **2024**, 759–785.
30. Collares, D.M. An Alternative Way to Look at Diffuse Large B-Cell Lymphoma: The Impact of Frequent Engagement of ReIB NF-KB Subunit on Cell Survival and Patient Outcome 2019.